Title

Ripples on spikes show increased phase-amplitude coupling in mesial temporal lobe epilepsy seizure-onset zones

Journal

Epilepsia, 57(11)

ISSN

0013-9580

Authors

Weiss, Shennan A
Orosz, Iren
Salamon, Noriko
et al.

Publication Date

2016-11-01

DOI

10.1111/epi.13572

Peer reviewed

FULL-LENGTH ORIGINAL RESEARCH

Ripples on spikes show increased phase-amplitude coupling in mesial temporal lobe epilepsy seizure-onset zones

*†Shennan A. Weiss, ‡Iren Orosz, ‡Noriko Salamon, *Stephanie Moy, *Linqing Wei, *§Maryse A. Van't Klooster, ¶#Robert T. Knight, **Ronald M. Harper, *Anatol Bragin, ††Itzhak Fried, ***‡‡§§Jerome Engel Jr, and *Richard J. Staba

Epilepsia, 57(11):1916–1930, 2016
doi: 10.1111/epi.13572

Dr. Shennan Aibel Weiss is an assistant professor at Thomas Jefferson University Department of Neurology; he recently completed his epilepsy fellowship at the University of California Los Angeles.

Summary

Objective: **Ripples (80–150 Hz) recorded from clinical macroelectrodes have been shown to be an accurate biomarker of epileptogenic brain tissue. We investigated coupling between epileptiform spike phase and ripple amplitude to better understand the mechanisms that generate this type of pathologic ripple (pRipple) event.**

Methods: **We quantified phase amplitude coupling (PAC) between epileptiform electroencephalography (EEG) spike phase and ripple amplitude recorded from intracranial depth macroelectrodes during episodes of sleep in 12 patients with mesial temporal lobe epilepsy. PAC was determined by (1) a phasor transform that corresponds to the strength and rate of ripples coupled with spikes, and a (2) ripple-triggered average to measure the strength, morphology, and spectral frequency of the modulating and modulated signals. Coupling strength was evaluated in relation to recording sites within and outside the seizure-onset zone (SOZ).**

Results: **Both the phasor transform and ripple-triggered averaging methods showed that ripple amplitude was often robustly coupled with epileptiform EEG spike phase. Coupling was found more regularly inside than outside the SOZ, and coupling strength correlated with the likelihood a macroelectrode's location was within the SOZ ($p < 0.01$). The ratio of the rate of ripples coupled with EEG spikes inside the SOZ to rates of coupled ripples in non-SOZ was greater than the ratio of rates of ripples on spikes detected irrespective of coupling ($p < 0.05$). Coupling strength correlated with an increase in mean normalized ripple amplitude ($p < 0.01$), and a decrease in mean ripple spectral frequency ($p < 0.05$).**

Significance: **Generation of low-frequency (80–150 Hz) pRipples in the SOZ involves coupling between epileptiform spike phase and ripple amplitude. The changes in excitability reflected as epileptiform spikes may also cause clusters of pathologically interconnected bursting neurons to grow and synchronize into aberrantly large neuronal assemblies.**

KEY WORDS: **Mesial temporal lobe epilepsy, High-frequency oscillation, Epileptiform discharge, Ripple, Intracranial EEG.**

Accepted August 29, 2016; Early View publication 10 October 2016.

*Department of Neurology, David Geffen School of Medicine at UCLA, Los Angeles, California, U.S.A.; †Department of Neurology, Thomas Jefferson University, Philadelphia, Pennsylvania, U.S.A.; ‡Department of Radiology, David Geffen School of Medicine at UCLA, Los Angeles, California, U.S.A.; §Department of Neurology and Neurosurgery, Brain Center Rudolf Magnus, University Medical Center Utrecht, Utrecht, The Netherlands; ¶Departments of Psychology and #Neuroscience, University of California Berkeley, Berkeley, California, U.S.A.; **Departments of Neurobiology, ††Neurosurgery, and ‡‡Psychiatry and Biobehavioral Sciences, David Geffen School of Medicine at UCLA, Los Angeles, California, U.S.A.; and §§Brain Research Institute, David Geffen School of Medicine at UCLA, Los Angeles, California, U.S.A.

Address correspondence to Shennan A. Weiss, 710 Westwood Plaza, Los Angeles, CA 90095-1769, U.S.A. E-mail: saweiss@mednet.ucla.edu

Key Points

- The phase of epileptiform spikes modulates the amplitude of pathologic ripples (pRipples, 80–150 Hz)
- The strength of this form of phase amplitude coupling is increased in the SOZ of patients with mesial temporal lobe epilepsy
- The strength and rate of coupling improved the precision of the pRipples for identifying the SOZ
- The strength of coupling was directly correlated with ripple amplitude and indirectly correlated with ripple spectral frequency
- Changes in excitability cause clusters of pathologically interconnected neurons to expand and synchronize generating pRipples

Mesial temporal lobe epilepsy (MTLE) is the most common adult form of medically refractory epilepsy and is often amenable to resective epilepsy surgery.[1] When the seizure-onset zone (SOZ) is unilateral and localized to the mesial temporal lobe, anteromesial temporal lobectomy is the recommended procedure, and up to 85% of patients are seizure free after surgery.[2,3]

Differentiating MTLE patients with a primarily unilateral SOZ from patients with SOZs that are bilateral independent, or also include neocortical regions, would be aided by a more precise interictal neurophysiologic biomarker of epileptogenic mesial temporal lobe brain tissue.[4] High-frequency oscillations (HFOs) are brief (15–200 msec) bursts of neurophysiologic activity that range in frequency between 80 and 600 Hz. They are considered a candidate biomarker of epileptogenic tissue in intracranial recordings.[5] The epileptogenic zone is not always congruent with the SOZ, and it may not be fully characterized due to spatial or limited duration of recordings by the intracranial electrodes during the epilepsy monitoring unit stay.[6]

Epileptogenic hippocampus and entorhinal cortex can be identified on the basis of increased interictal high-frequency (fast) ripple (200–600 Hz) burst rates in experimental microelectrode recordings, but not usually HFO bursts of lower frequency ripples (80–200 Hz).[7–9] High frequency, or fast ripples, are believed to reflect summated action potentials from clusters of synchronously bursting pathologically interconnected neurons,[10] whereas sharp-wave ripples in normal hippocampus are considered important for memory encoding, consolidation, and recall,[11–14] and reflect summated inhibitory postsynaptic potentials.[15,16] However, in the epileptic brain, some ripple frequency oscillations are pathologic, and clinical macroelectrode recordings show that increased rates of both interictal ripples and fast ripples delineate the SOZ.[17,18]

Epileptiform spikes are usually distinct in morphology, higher in amplitude, and shorter in duration compared to physiologic sharp waves.[19] Thus ripples that occur during epileptiform spikes are likely to be pathologic, and not normal phenomenon, that is, pathologic ripples (pRipples). The underlying mechanisms that generate low-frequency (80–150 Hz) pRipples on spikes have not yet been fully elucidated. We hypothesize that these pRipples may be generated when the changes in excitability that are reflected as epileptiform spikes, also cause growth and synchronization of clusters of pathologically interconnected bursting neurons in epileptogenic regions. Synchronizability of the neuronal assembly[20] should manifest as coupling between the epileptiform spike phase and the ripple amplitude,[21,22] since the changes in excitability are related to the spike phase.

In the current study, we quantified coupling between the epileptiform spike phase and ripple amplitude in the interictal depth electrode electroencephalography (EEG) recordings from presurgical patients with drug-resistant seizures, and asked if this form of phase-amplitude coupling was associated with the SOZ. We also determined whether the strength of this coupling influenced ripple amplitude and frequency. We performed computer-aided visual inspection of the intracranial EEG (iEEG), a novel phasor transform methodology, and ripple-triggered averaging measures that derive the waveform and strength of the modulatory signal.

Methods

Patient selection

The 12 patients involved in this retrospective study underwent depth electrode evaluation at the University of California Los Angeles (UCLA) Seizure Disorder Center between 2010 and 2016, and were selected on the basis of (1) availability of interictal recordings with a 2 kHz sampling rate, and (2) a mesial temporal lobe SOZ, confirmed by bilateral depth macroelectrode recordings.

Localization of electrode sites and three-dimensional reconstructions

All patients were scanned preimplantation using a 3T magnetic resonance imaging (MRI) scanner (Magnetom; Siemens Trio, Erlangen, Germany), with a protocol consisting of at least a T_1-weighted magnetization prepared rapid aquisition gradient echo (MPRAGE) sequence. For some patients, postresection scans were also performed. Postimplantation computerized tomography (CT) scans contained signal artifact corresponding to the contacts of all implanted depth electrodes. CT images were nonlinearly and manually coregistered to the preimplantation and postresection T_1-weighted images using FMRIB's linear image registration tool (FLIRT) (http://fsl.fmrib.ox.ac.uk/fsl/fslwiki/FLIRT). Each individual intracranial macroelectrode contact was manually delineated using the AFNI program (https://afni.nimh.nih.gov/afni/). Freesurfer software (http://freesurfer.net/) was used to segment brain structures and cortical surfaces, and the three-dimensional (3D) images were

displayed using Slicer (https://www.slicer.org/). To differentiate macroelectrode contacts residing in gray or white matter, the preimplantation T_1-weighted MRI was anatomically segmented into 94 gray and white matter regions of interest using BrainSuite (http://brainsuite.org) and verified via visual inspection.

Recording methods and selection of data

Clinical iEEG (0.1–600 Hz; 2,000 samples per second; reference scalp Fz) was recorded from 7-contact depth electrodes (Ad-Tech Medical Instrument Corp., Racine, WI, U.S.A.) using a Stellate (XLTEK, San Diego, CA, U.S.A.) or a Nihon-Kohden 128-channel NK 1200 long-term monitoring system (Nihon-Kohden America, Foothill Ranch, CA, U.S.A.). The recordings were acquired during a 35–60 min epoch of mixed-stage sleep. Sleep was confirmed by video-EEG inspection revealing K-complexes, spindles, slow waves, and a paucity of muscle artifact. We did not perform concurrent electrooculography (EOG) and electromyography (EMG) recordings. Antiseizure drug blood serum levels at the time of the recording were not available. The SOZ was defined by a consensus decision made among a team of board-certified epileptologists on the basis of visual inspection of the iEEG using the criteria of identifying the electrodes first exhibiting the ictal-onset pattern.[23]

HFO detection and quantification

Muscle and electrode artifacts in iEEG recordings were reduced using a custom independent component analysis (ICA) based algorithm (Appendix S1, Fig. S1). After applying this ICA-based method, ripples were detected in the referential montage iEEG recordings per macroelectrode contact by utilizing a Hilbert-detector methodology (Appendix S1, Fig. S1).

Distinguishing ripples on spikes and reducing ringing artifact

To distinguish ripples that occur during epileptiform spikes from all other ripples, we calculated the derivative of the peri-ripple band-pass filtered (4–30 Hz) iEEG and applied a threshold of 2 μV/msec. Ripple events that exceeded this threshold were inspected and categorized as ripples on spikes (Fig. S1).

Oscillatory events can arise due to Gibb's phenomenon as a result of high-pass filtering sharp transients such as an epileptiform spike.[24] We developed a custom algorithm to exclude these events (Appendix S1, Fig. S3). The performance of this method was confirmed with visual inspection.

Quantifying ripple detection accuracy

In a subset of the macroelectrode recordings (N = 4 patients) the detector results were used to annotate the iEEG recording and were compared to the gold standard of visual inspection. The overall sensitivity of the detector for ripples events during epochs containing artifact was 96.7 ± 2%, and the overall precision of the detector was 88.7 ± 6.5%.

The ratio of the ripple rates detected from macroelectrodes positioned in gray matter relative to the ripple rates detected from macroelectrodes in white matter was 4.03 ± 1.9 (n = 7, paired Student's *t*-test $p < 0.05$).

Utilization of ripple phasors

To examine and quantify coupling between spike phase and ripple amplitude, we transformed each ripple on spike event into a ripple phasor calculated on the basis of the instantaneous phase $\phi(t)$ of the low frequency iEEG recording and the corresponding instantaneous amplitude a(t) during the duration of the ripple event (Fig. S2).

Each ripple phasor was calculated using Equation 1:

$$ve^{i\theta} = \sum_{t}^{T} a(t)e^{i\phi(t)}, \quad (1)$$

where v is the vector strength of the phasor, theta its phase angle, and a(t) and $\phi(t)$ are the respective instantaneous ripple amplitude and low frequency iEEG phase during the ripple across its duration [t..T] (Fig. S2).

Phase locking among the multiple HFO phasors [n..N] detected from individual macroelectrodes was performed using Rayleigh's test for circular nonuniformity by calculating the mean vector strength (r) using Equation 2.

$$r = \frac{|\sum_{n}^{N} v_n e^{i\theta_n}|}{\sum_{n}^{N} v_n}, \quad (2)$$

and deriving the Rayleigh Z-statistic Equation 3.

$$Z = Nr^2. \quad (3)$$

Rayleigh's test for circular nonuniformity assumes a null hypothesis of uniformity (or bimodal opposing directions), and is based on determining the mean phase angle and angular spread across the individual phasors.

We calculated the phase-locked ripple phasor rate on the basis of (1) identifying electrodes in which the ripple phasors for all the detected ripple events exhibited statistically significant phase locking (Rayleigh's test for circular nonuniformity, $p < 0.05$) and (2) tallying the number of ripple phasors that were within ±90 degrees of the mean phase angle of the total population of ripple phasors. By convention, 0 degrees is the peak of an oscillation, and 180 degrees is the trough.

Ripple-triggered averaging

To identify and characterize the low-frequency waveforms and oscillations that modulate ripple amplitude, we

used a ripple-triggered coupling methodology.[25] Trials of unfiltered iEEG, 1 s in duration, aligned by the time of the maximum instantaneous amplitude of the ripple events at 0.5 s were summated to derive a modulatory signal. The statistical significance of the modulatory signal was derived by computing 300 surrogates using phase shuffling, and calculating the peak-to-peak amplitude of the randomized signals. The modulated signal was calculated by convolving each 1 s unfiltered iEEG trial, with a ripple occurring at ~0.5 s, with complex Morlet wavelets with a width of seven cycles, and a standard deviation of three cycles using Fieldtrip (http://www.fieldtriptoolbox.org/). The time-frequency representations for each trial were then averaged and normalized (using a z-score) to account for (1/f) spectral power.

Statistics

The SOZ rate ratio for ripple events and phase-locked ripple phasor events was calculated using Equation 4.

$$rr_{SOZ} = \left(\frac{\text{Mean Event Rate}_{SOZ} - \text{Mean Event Rate}_{NSOZ}}{\text{Mean Event Rate}_{SOZ} + \text{Mean Event Rate}_{NSOZ}}\right). \quad (4)$$

The correlation between ripple rates, Rayleigh score, and phase-locked ripple rates and the likelihood an electrode was positioned in the SOZ was calculated by (1) rank ordering of the rates and scores within each subject, (2) assigning the rank-ordered electrode a binary value based on its location, (3) summating these assigned values for the rank-ordered channels across patients, and (4) performing a linear regression analysis between rank order and the resulting SOZ probability. Paired and unpaired student's *t*-tests were two tailed, with a 0.05 significance level. The Kuiper's test was performed using the circular statistic toolbox in Matlab (http://www.mathworks.com/matlabcentral/fileexchange/10676-circular-statistics-toolboxdirectional-statistics-).

Results

Description of patients and recordings

Patients with suspected temporal lobe epilepsy during scalp EEG in the epilepsy monitoring unit were selected for depth electrode EEG monitoring due to (1) bilateral interictal and ictal findings, (2) a normal brain MRI or positron emission tomography (PET) study, or (3) concern for a possible lateral temporal SOZ (Table 1). Only 12 of these patients were included in this study due to the availability of 30 min of artifact-free interictal recordings sampled at 2 kHz during sleep. We analyzed recordings from between 2 and 9 macroelectrode contacts on 7–10 depth electrodes per patient (Table 1). We did not analyze recordings from every macroelectrode contact due to excessive artifact that interfered with HFO detection. Overall, across the 12 patients, recordings from 640 distinct macroelectrode contacts were analyzed. Of the 640 distinct macroelectrode recordings, 147 were located in the SOZ.

Of the 12 patients, a diagnosis of unilateral mesial temporal SOZ was made in three patients; bilateral mesial temporal SOZ in four patients; mesial and lateral (i.e., neocortical) temporal SOZ in four patients; and mesial, lateral temporal, and extratemporal SOZ in one patient. All three patients with unilateral MTLE were offered an anterior temporal lobectomy, but conclusive postresection seizure outcomes are not yet available (Table 1). One patient had a mesial temporal and temporal neocortical SOZ and was seizure free after a mesial and neocortical resection, whereas another had independent SOZs in the right and left mesial temporal structures, but underwent a palliative right anterior temporal lobectomy with an Engel class II outcome.

Ripple amplitude is coupled with epileptiform spike phase

Visual inspection of the iEEG recordings demonstrated that ripples could occur with or without epileptiform EEG spikes (Fig. 1A,B). Using the recordings from all 640 macroelectrodes, we detected a total of 28,957 ripples, and of these, 14,502 ripples were associated with an epileptiform spike. For each ripple, we calculated a "ripple phasor" (Figs. S1 and S2), a new measure that corresponds to the magnitude and phase angle between the instantaneous amplitude of the band-pass (80–150 Hz) filtered ripple and the instantaneous phase of the Hilbert-transformed, band-pass (4–30 Hz) filtered epileptiform spike or low-frequency EEG in the absence of an epileptiform spike (Fig. 1C1,C2). In many cases, ripple phasors indicated that ripples occurred within a relatively narrow range of phase angles when associated with an epileptiform spike (Fig. 1C1), compared to when ripples occurred in the absence of a spike (Fig. 1C2). Subsequently, for each macroelectrode we determined if all the ripples on spikes (RonS) transformed to phasors were phase-locked (Fig. 1D1, Rayleigh's test for circular non-uniformity, $p < 0.05$). If the ripple phasors exhibited phase locking, we tallied the number of ripple phasors with a respective phase angle within ±90 degrees of the mean phase angle of the distribution (i.e., phase-locked ripple phasors).

To verify the strength of coupling indicated by the ripple phasor methods, as well as the spectral frequency profile, we calculated the ripple-triggered average to evaluate the modulating signal (i.e., epileptiform spike) and the mean time-spectral frequency representation of the ripples. In the analysis of macroelectrode recordings that exhibited phase-locked ripple phasors, the maximum ripple amplitude occurred near either the peak (Fig. 2A1,A2) or the trough (Fig. 2A3,A4) of the epileptiform spike. In 13 of 16 of the

Table 1. Patient characteristics

Patient Age Sex	Sleep stage	Scalp EEG	MRI	PET hypometabolic	iEEG macro electrode sites	iEEG IED	iEEG SOZ	Surgery	Path	Outcome
1 34 M	SWS Delta = 92%	IEDs L(T1) > R(T2), SOZ L(T1, T3)	Normal	Bitemporal	RA1-7 RAH1-7 REC1-7, RPHG1-7 ROF1-7 LA1-7 LAH1-7 LEC1-7 LPHG1-7 LOF1-7	L = R MT/LT	L MT > R MT/LT	None	N/A	N/A
2 54 F	1,2 Delta = 89%	IEDs R(T4), SOZ R(T2, T4)	Normal	R. temporal	RA1-6 RMH2-6 RSTa1-3 RSTp2-5 RSS1-9 RIPa1-7 RIPp1-9 LMH1-5	R LT	R MT/LT	R. MT, LT resection	Gliosis	Engel class I at 4 years
3 52 F	1,2 SWS Delta = 95%	IEDs L(T1), SOZ L(T1) > R(T2)	Normal	Normal	RA1,2,4-7 RMH1-6 ROF1,5-7 LA1-6 LEC1-7 LMH1-6 LOF1-6	R > L MT	R ≫ L MT	R. ATL	FCD Ic	Engel class II at 3 years
4 53 M	1,2 Delta = 85%	IEDs L(T1), SOZ L(broad)	L. PCA infarct	L. PCA territory	REC1-7 RPHG1-7 LA1-6 LEC1,2-4-7 LFSG1-3 LOTa1,2 LTOp3-5 LSO2-3	L MT > LT	L MT	L. ATL	Gliosis	Deceased
5 47 F	A,1,2,SWS Delta = 85%	IEDs L(T1) = R(T2), SOZ L(T1) > R(T2)	R inf. frontal abnormality	L > R temporal	RAH1-7 REC1-4,6-7 ROF1-7 RPAR1-7 RAC1-7 LAH1-7 LEC1-7 LOF1-7 LAC1-7	R > L MT	R > L MT	None	N/A	N/A

Continued

Epilepsia, 57(11):1916–1930, 2016
doi: 10.1111/epi.13572

Table 1. Continued.

Patient Age Sex	Sleep stage	Scalp EEG	MRI	PET hypometabolic	iEEG macro electrode sites	iEEG IED	iEEG SOZ	Surgery	Path	Outcome
6 42 F	A,1,2 Delta = 85%	IEDs R(T2) > L(T1), SOZ L(T3) > R(T2)	T2/FLAIR hyperintense R. temporal pole	R temporal pole	RA2-7 REC1-7 RMH2-7 RPHG1-7 ROF1-7 LA2-7 LEC1-3,5-7 LAH2-7 LPHG4-7	L > R MT	R MT	R. ATL	FCD IIb	No seizures at 6 months
7 35 F	1,2 Delta = 76%	IEDs R(T4) > R(T2), SOZ R(T4)	s/p RNS removal	R temporal	RA1-7 REC1-6 RMH2-6 ROF1-6 RAC1-7 SMA2-3 RMC1-7 LEC1-6 LMH3-5	R MT	R MT > LT	R. ATL	Gliosis	Seizures continue at 6 months
8 35 F	1,2 Delta	IEDs R(T4) > L(T3) SOZ, R(T2), R(T4), left broad PFA	R > L peri-ventricular heterotopia cingulate polymicrogyria, hypothalamic hamartoma	L > R temporal, and periventricular	REC2-6 RMH1-7 ROF1-7 RTO1-7 LA1-7 LEC2-6 LMH2-7 LPHG1-7 LTO1-3,5-7	R MT	R MT/LT, L LT, R O	None	None	N/A
9 30 M	1,2 Delta = 80%	IEDs L(T1) = R(T2) SOZ, R(T2)	Normal	R lateral i.e., (neo) temporal	RA1-7 REC1-7 RMH1-7 RPHG1-6 RSTG1-7 ROF1-7 RAC1-7 LEC1-7 LAH1-7	L > R MT	R > L MT	None	N/A	N/A
10 27 M	1,2 Delta = 89%	IEDs L(T1) = R(T2) SOZ, R(T4) = L(T1)	R parietal resected AVM, R MTS	R mesial temporal	RA1-6 REC1-6 RMH1-6 RPHG1-7 LEC1-6	R > L MT	R > L MT	None	N/A	N/A

Continued

Table 1. Continued.

Patient Age Sex	Sleep stage	Scalp EEG	MRI	PET hypometabolic	iEEG macro electrode sites	iEEG IED	iEEG SOZ	Surgery	Path	Outcome
					LMH1-6					
					RPC1-7					
					RTO1-6					
					RO1-4					
11	2, SWS	IEDs	Right	Right	REC1-6	R MT = R LT	R MT/LT	R ATL	TBD	TBD
30	Delta	R(T2, T4)	orbitofrontal	orbitofrontal	RAH1-7					
F	–	SOZ	volume loss		RPHG1-7					
	82%	R(T2, T4)			RSTG1-7					
					RA1-6					
					ROF1-5,7					
					RAF1-5,7					
					LEC1-7					
					LMH1-6					
12	2, SWS	IEDs, L(T1)	Left anterior	L. temporal	RAH3-7	L > R MT	L MT	L ATL	TBD	TBD
21	Delta	SOZ	temporal		REC1-7					
F	83%	L(F7, T1)	encephalocele		RPHG1,2,5-7					
					ROF1-5					
					LA1-4,6-7					
					LEC1-7					
					LMH1-7					
					LPHG1-7					

A, awake; 1, stage 1 sleep; 2, stage 2 sleep; SWS, slow wave sleep; L, left; R, right; IEDs, interictal epileptiform discharges; SOZ, seizure-onset zone; AVM, arteriovenous malformation; MTS, mesial temporal lobe sclerosis; A, amygdala; AH, anterior hippocampus; MH, middle hippocampus; EC, entorhinal cortex; PHG, parahippocampal gyrus; FSG, fusiform gyrus; STa, superior temporal (anterior); STp, superior temporal (posterior); SS, superior temporal sulcus; OF, orbitofrontal; AC, anterior cingulate; PC, posterior cingulate; IPa, inferior parietal (anterior); IPp, inferior parietal (posterior); PAR, parietal; OTa, occipital-temporal (anterior); TOP, temporal-occipital (posterior); SO, superior occipital; SMA, supplementary motor area; MC, middle occipital; TO, temporal occipital; O, occipital; RNS, repetitive nerve stimulator; FLAIR, fluid attenuated inversion recovery; PCA, posterior cerebral artery; MT, mesial temporal intracranial electrodes; LT, lateral (i.e., neocortical) temporal intracranial electrodes; O, occipital; ATL, anterior temporal lobectomy; FCD, focal cortical dysplasia; TBD, to be determined; N/A, not applicable.

Scalp EEG findings provide the laterality and relative frequency of IEDs and seizures, as well as the electrode (in parenthesis) where interictal discharges or seizures are maximal or phase reverse. Intracranial findings provide the localization and relative frequency of interictal discharges and seizures.

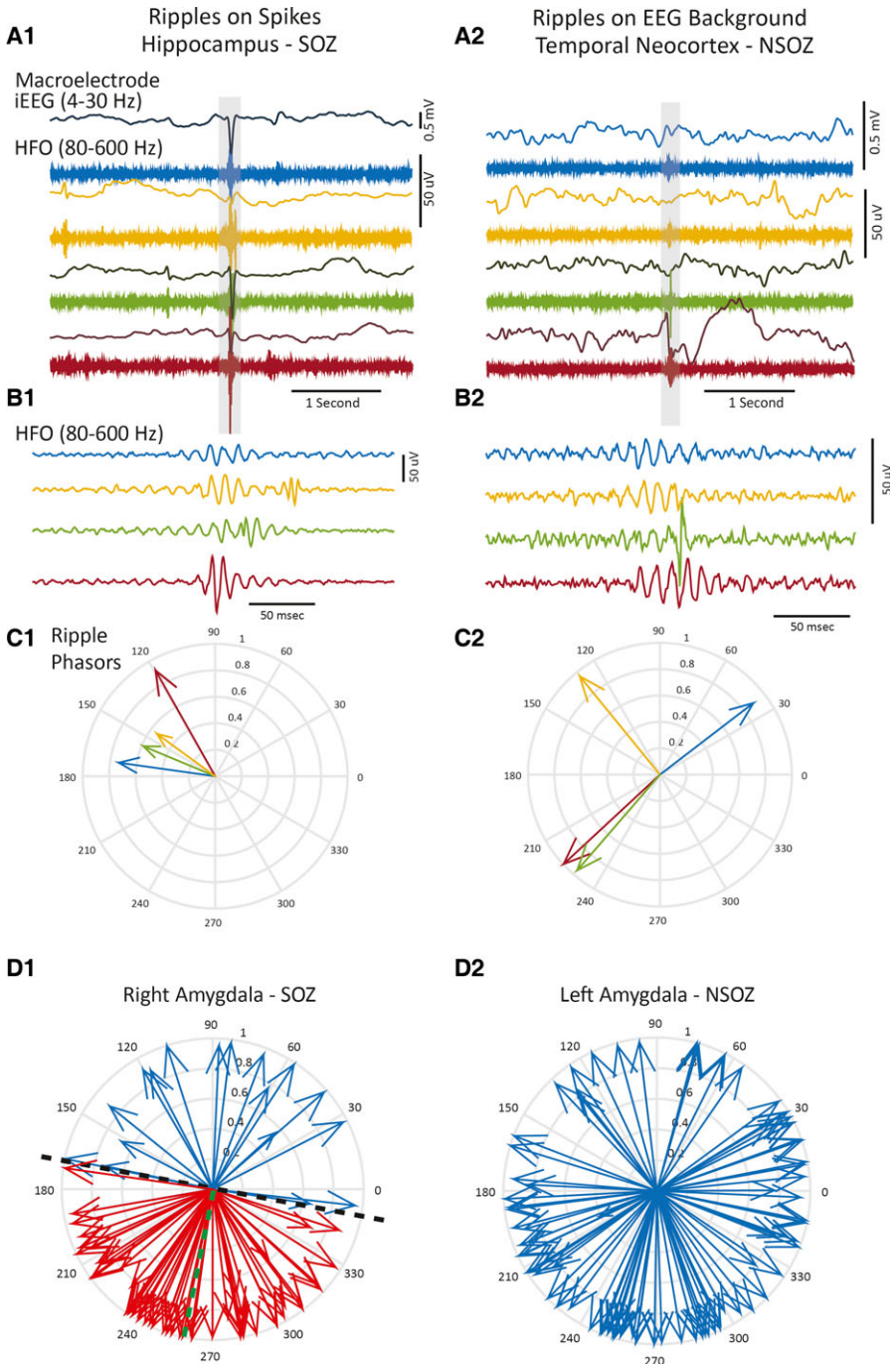

Figure 1.

Ripples can occur during epileptiform spikes or superimposed on the background EEG. (**A**) Four examples of the band-pass filtered (4–30 Hz, top) EEG and corresponding band pass (80–600 Hz, middle) for ripples recorded from the hippocampus in the SOZ (left) and neocortical temporal contact (right) located contralateral to the SOZ. The traces are aligned to ripple events (gray bar). The ripples recorded from the hippocampus occurred during interictal epileptiform EEG spikes, whereas neocortical ripples occurred during absence of EEG spikes. (**B**) Expansion of the aligned HFOs illustrated by the gray bar in **A**. (**C**) Polar plot of color-coded ripple phasors corresponding to ripples illustrated in panels **A** and **B**. Note the narrow range of phase angles associated with ripples associated with EEG spikes compared to ripples that occurred in the absence of EEG spikes. (**D**) Polar plots of the ripple phasors (blue) and phase-locked ripple phasors (red) for events recorded from the right amygdala in the SOZ (**D1**); green dashed line represents the mean phase angle of all the phasors, dashed black line represents the division between phase locked (red) and non–phase-locked ripple phasors. The coupling strength of the ripple phasors recorded from the left amygdala in the NSOZ was comparatively weaker (**D2**).

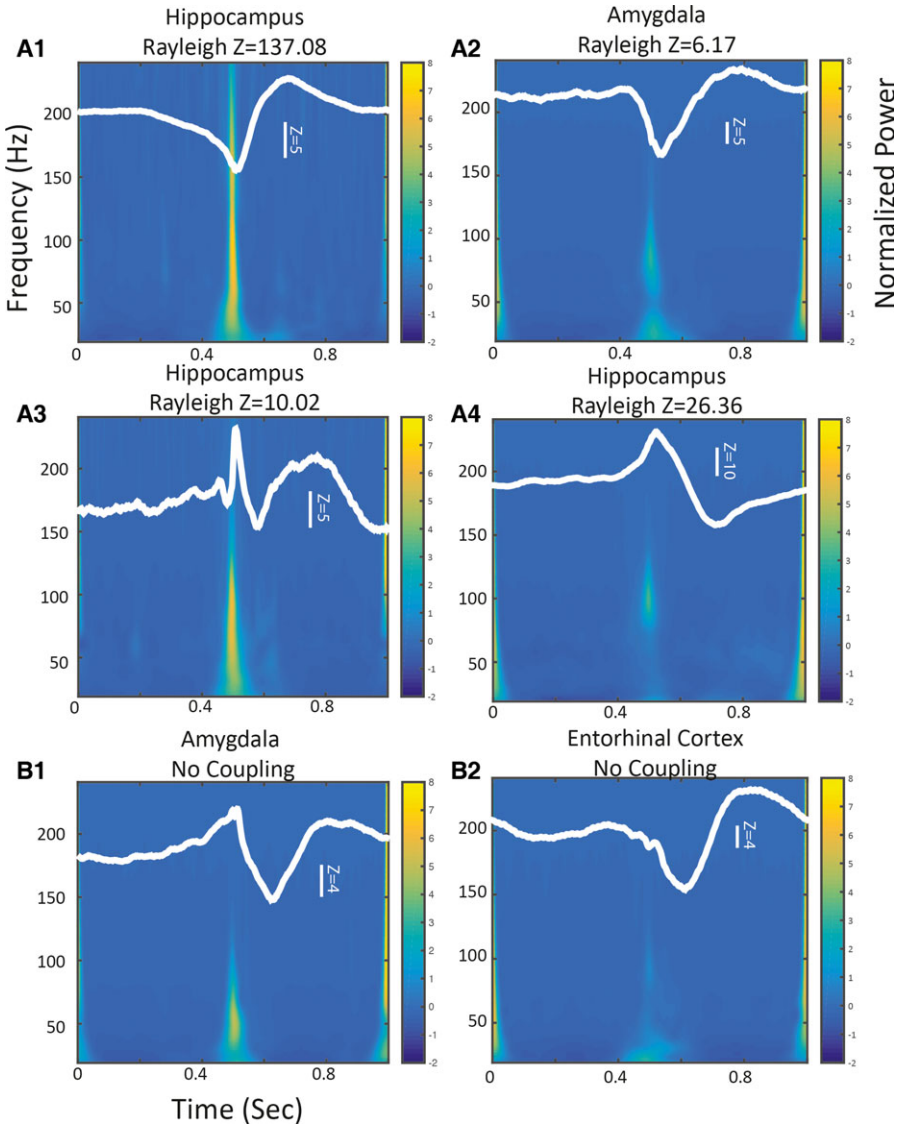

Figure 2.

Ripple-triggered averaging demonstrates that ripple and gamma amplitude is coupled with the epileptiform spike. The unfiltered iEEG during ripples was aligned temporally with the maximum ripple amplitude, the resulting ripple-triggered averaged signal (white trace) had a peak-to-peak amplitude corresponding to the strength of coupling and a phase at time 0.5 s corresponding to the preferred phase of coupling. The superimposed normalized averaged time-frequency representation of the aligned unfiltered ripple events was calculated by wavelet convolution. (**A**) Ripple-triggered averaging results are shown for four electrodes that exhibited phase-locked ripple phasors. In example **A1** and **A2,** the preferred phase angle of coupling is near the trough of the epileptiform spike; in examples **A3** and **A4** the preferred phase angle is near the peak. In **A1**–**A3,** epileptiform spike phase is also coupled with gamma amplitude as well as ripple amplitude. (**B**) Ripple-triggered averaging results for two electrodes that did not exhibit phase-locked ripple phasors. Note the weaker coupling and absence of well-defined ripple power at the preferred phase.

macroelectrodes, gamma amplitude as well as ripple amplitude was coupled with the epileptiform spike (Fig. 2A1–A3); however, in the other three macroelectrode recordings, only ripple amplitude was coupled to the peak of the epileptiform spike (Fig. 2A4). By contrast, in macroelectrode recordings that contained high rates of ripples that were not phase locked with spikes, the corresponding ripple-triggered averaging analysis showed a weak modulating signal (Fig. 2B1) and relatively reduced ripple power during the epileptiform spike (Fig. 2B2).

Coupling between epileptiform spike phase and ripple amplitude is increased in the SOZ

Across the 12 patients, ripple phasors derived from RonS were phase locked in 93 (63.3%) of 147 macroelectrodes in the SOZ, and 137 (27.8%) of 493 of the macroelectrodes in

the NSOZ. In certain patients, ripple rates were elevated both in the SOZ and NSOZ, but phase-locked ripple rates were elevated exclusively in the SOZ (Fig. 3).

An analysis of ratios of total ripple occurrence in the SOZ to total ripple occurrence in NSOZ showed ratios >0 in all patients (Fig. 4A). Similarly, ratios derived from the rates of RonS irrespective of coupling were also >0, but in most patients, the highest ratios were those calculated from the phase-locked ripple phasors (Fig. 4A, Student's paired *t*-test, n = 12, $p < 0.05$). The rates of total ripples, RonS, and phase-locked ripple phasors were also higher in the SOZ electrodes compared to respective rates in the NSOZ electrodes (Fig. S4, Student's paired *t*-test, n = 12, $p < 0.01$). On the basis of visual review of several days of

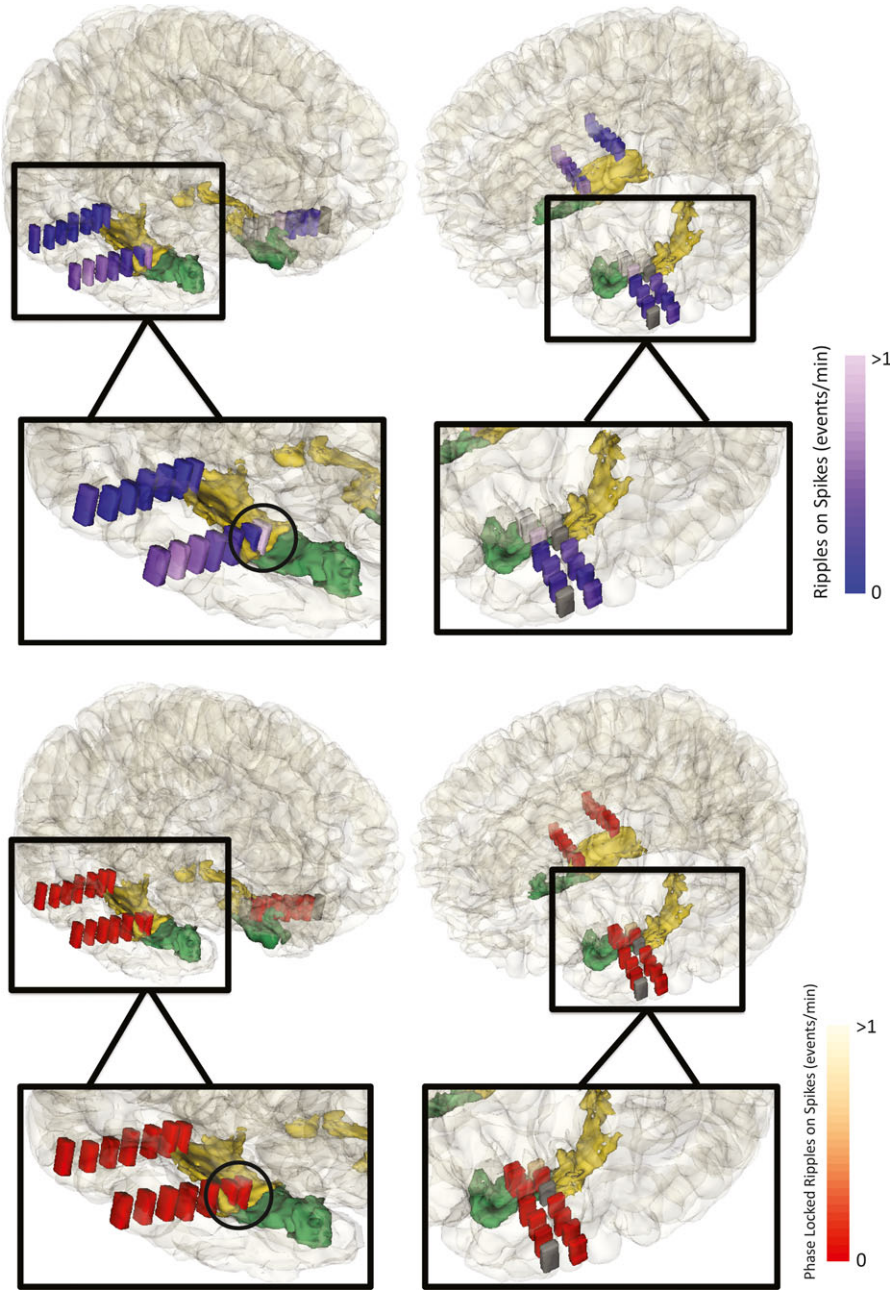

Figure 3.
Ripples on spikes that are transformed to phasors can unambiguously lateralize the mesial temporal seizure-onset zone (SOZ). Coregistered CT-MRI of patient 4 with a left mesial temporal SOZ; the rates of ripples on spikes are shown in blue (above), and the rate of the phase-locked ripple phasors after transforming the ripples on spikes are shown in red (below). Dark gray macroelectrodes indicate contacts excluded due to poor recording quality.

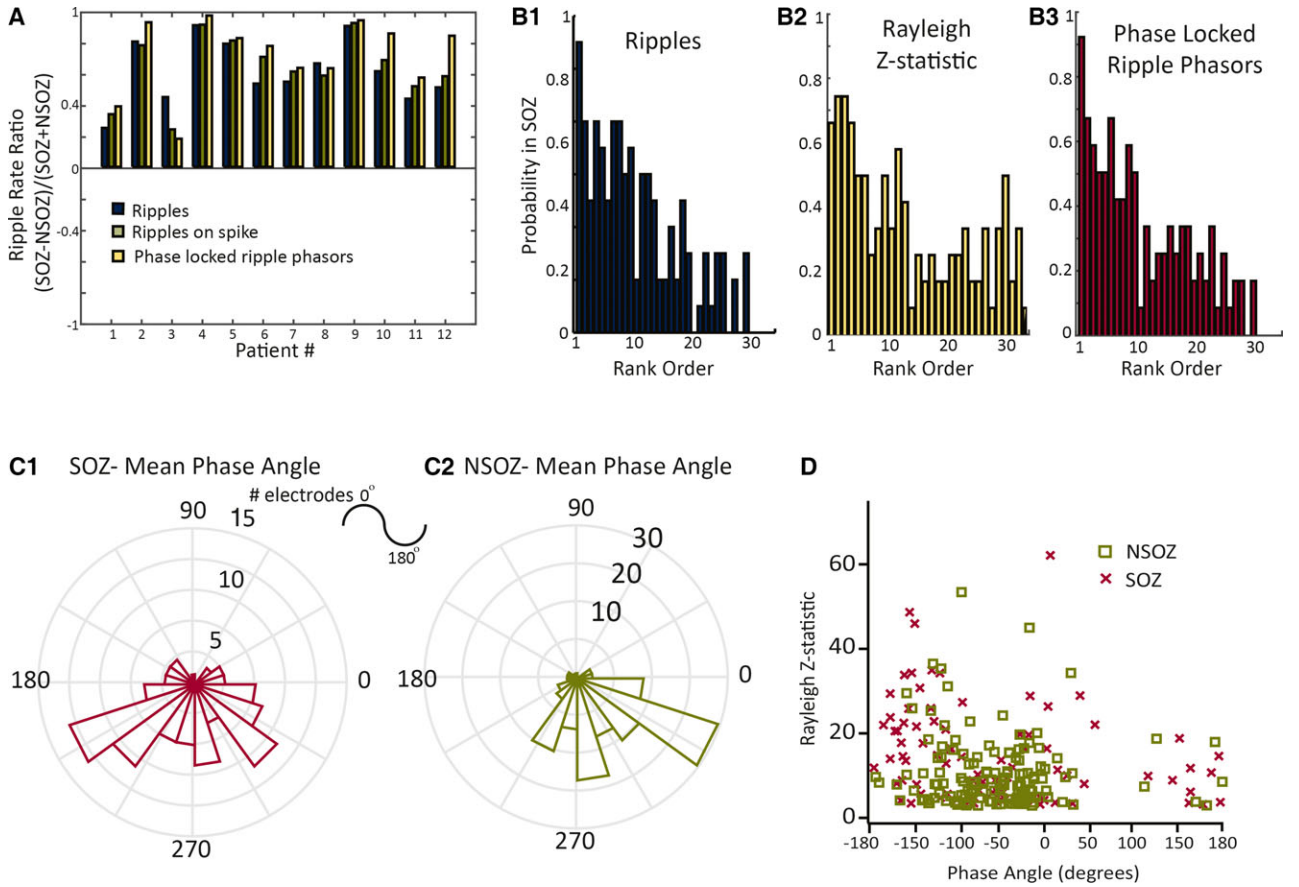

Figure 4.

Coupling between epileptiform spike phase and ripple amplitude can be used to identify the seizure-onset zone. (**A**) The ripple rate ratio calculated on the basis of mean event rates measured from electrodes in the SOZ, and non-SOZ (NSOZ). Both raw ripples, ripples on spikes, and ripples on spikes transformed to phase-locked ripple phasors were overly represented in the SOZ in all 12 patients. Across the 12 patients, the SOZ rate ratio for phase-locked ripple phasors (yellow) exceeded the ratio for ripples (blue), and ripples on spikes (Student's paired *t*-test, n = 12, $p < 0.05$). (**B**) Comparison between rank-ordered total rate of ripple occurrence (**B1**), rank-ordered Rayleigh Z-statistic for the phase- locked ripple phasors (**B2**), and rank-ordered of rate of phase-locked ripple phasors (**B3**) and the probability that a given macroelectrode lay within the SOZ. (**C**) Polar histogram of the mean phase angle of the ripples on spikes transformed to phase-locked ripple phasors measured in the SOZ (red, **C1**) and the NSOZ (green, **C2**). (**D**) Scatter plot of the mean phase angle and Rayleigh Z-statistic of these ripple phasors identified in electrodes in the SOZ (red), and in the (NSOZ).

iEEG recording, interictal epileptiform discharges (IEDs) also occurred at a higher rate in the SOZ in the majority of patients (Table 1). However, in patients 6 and 11, IED rates were greater or equal in the mesial temporal lobe electrodes contralateral to the SOZ, respectively, whereas ripple rates were greatest in the SOZ electrodes.

The differences in mean ripple rates in the SOZ and NSOZ do not explicitly assess how the rate at individual electrodes accurately delineates the SOZ. To examine this question in more detail, we correlated the rank-ordered ripple rates with SOZ probability. Analysis showed a higher total ripple rate correlated with increased probability that the electrode was located in the SOZ ($R^2 = 0.66$, $p < 0.001$, n = 30; Fig. 5B1). In 11 of the 12 patients, the macroelectrode with the highest ripple rate was observed inside the SOZ (Fig. 4B1). Similarly, we evaluated the rank-ordered Rayleigh's Z-statistic, a measure of phase-locking strength, in relation to the SOZ. We found a larger Z-statistic correlated with increased likelihood the recording sites was in the SOZ ($R^2 = 0.44$, $p < 0.001$, n = 30; Fig. 4B2). Finally, our analysis showed that higher rates of phase-locked ripple phasors—which combine aspects of rate of occurrence and coupling strength—correlated with a greater likelihood that the recording sites were in the SOZ ($R^2 = 0.67$, $p < 0.001$, n = 30; Fig. 4B3).

We also examined if the properties of coupling between the phase of the epileptiform spike and ripple amplitude differed between electrodes located in the SOZ and NSOZ. Polar histograms of the mean phase angle of the phase-locked ripple phasors measured across all the macroelectrodes located in the SOZ revealed a preferred phase angle just after the trough of the epileptiform spike and

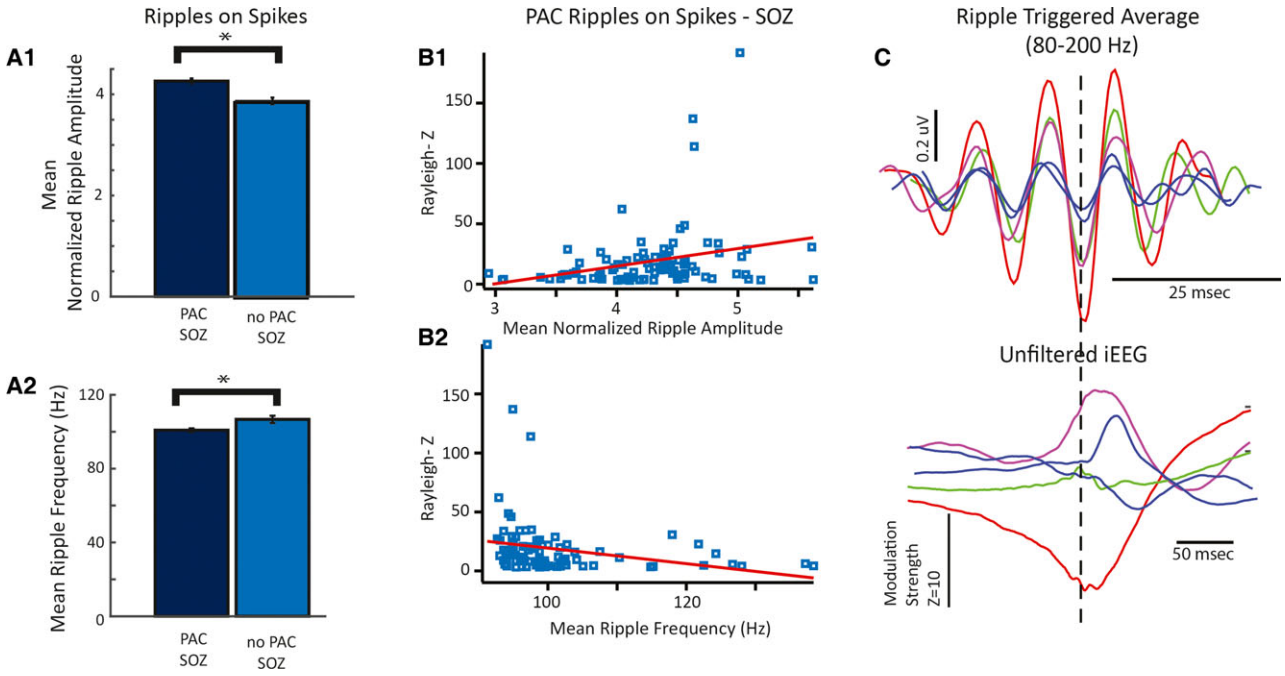

Figure 5.

The strength of coupling between epileptiform spike phase and ripple amplitude is positively correlated with mean ripple amplitude and negatively correlated with mean ripple frequency. In recordings from macroelectrodes in the SOZ, the presence of coupling between epileptiform phase and ripple amplitude (PAC) was associated with a greater mean normalized ripple amplitude (**A1**), and a decreased mean ripple frequency (**A2**) (Student's unpaired *t*-test, n = 93, 54 electrodes, $p < 0.01$, error bars = standard error of the mean [SEM]). (**B**) Among the recordings from macroelectrodes in the SOZ that exhibited PAC, the strength of coupling was associated with increased mean normalized ripple amplitude (**B1**, $R^2 = 0.0742$, d.f. = 92, $p < 0.01$) and decreased mean ripple frequency (**B2**, $R^2 = 0.053$, d.f. = 92, $p < 0.05$). (**C**) Illustrative examples of mean ripple-triggered averaged waveforms prior to (bottom) and after band-pass filtering (80–200 Hz; top) demonstrating relationship between modulation strength and ripple amplitude and frequency.

during the upstroke (Fig. 4C1), whereas, in the NSOZ, the preferred phase angle approached the peak of epileptiform spike (Fig. 4C2). Comparing the Rayleigh Z-statistic with the mean phase angle for each macroelectrode revealed that phase-locking strength was greatest when the mean phase angle was near the peak or the trough of the epileptiform spike (Fig. 4D). Across adjacent macroelectrodes positioned in mesial limbic structures, the preferred phase angle of ripple coupling to spikes shifted by over 75 degrees in ~30% of cases. When this phase shift occurred, the ripples recorded by the most-mesial hippocampal and entorhinal cortex contact were coupled with the peak of the epileptiform spike. Phase shifts >150 degrees were observed when comparing the preferred phase angle of coupling measured from contacts in mesial limbic structures with that measured from distal electrodes located in neocortex on the same depth probe in ~66% of cases. No phase shifts were evident for adjacent electrodes positioned in white matter.

The strength of coupling between epileptiform spike phase and ripple amplitude influences ripple properties

We asked if the spectral frequency and amplitude of ripples differed between ripples significantly coupled with epileptiform spikes and those that were not coupled. In the SOZ, we found that ripples coupled with epileptiform spikes exhibited a greater normalized mean amplitude (4.26 ± 0.05 vs. 3.87 ± 0.06, Fig. 5A1) and lower mean spectral frequency (100.83 ± 0.97 vs. 106.71 ± 1.97 Hz, Fig. 5A2), compared to the ripples uncoupled with epileptiform spikes (Student's unpaired *t*-test, n = 93, 54 electrodes, $p < 0.01$). There was no correlation between mean amplitude and spectral frequency ($R^2 = 0.0023$, d.f. = 92, $p < 0.65$). However, increased coupling strength correlated with larger mean normalized ripple amplitude (Fig. 5B1, $R^2 = 0.0742$, d.f. = 92, $p < 0.01$), and lower mean ripple spectral frequency (Fig. 5B2, $R^2 = 0.053$, d.f. = 92, $p < 0.05$). Finally, ripple-triggered averages showed greater modulation strength of the epileptiform spike correlated with higher ripple amplitude and lower ripple spectral frequency (Fig. 5C). In 3 of the 12 patients with both postresection MRI and outcome data available, we asked if ripples coupled with spikes exhibited different properties in the resected and unresected regions. We found that in patients 2 and 6, with seizure-free outcomes following resection, mean ripple coupling strength was increased, and spectral content was slightly decreased in the resected region, compared to the unresected regions

(Fig. S5). We did not observe differences in ripple amplitude.

Discussion

The major novel findings from this study show the following: (1) robust coupling between the phase of epileptiform spikes and the amplitude of ripples, (2) evidence that this form of phase-amplitude coupling is increased in strength in the SOZ, and (3) increased coupling strength correlates with ripples larger in amplitude and of a relatively lower spectral frequency.

Epileptiform spike phase is coupled to ripple amplitude

We used a new ripple phasor method and conventional event-triggered averaging to demonstrate that epileptiform spike phase is coupled to ripple amplitude. Both methods were in general agreement and found phase amplitude coupling (PAC) in the macroelectrode iEEG recordings.

Coupling between epileptiform spike phase and ripple amplitude is not equivalent to other forms of PAC described in the literature.[26] For example, in the human neocortex, robust coupling is evident between the phase of theta oscillations and the amplitude of high gamma oscillations. This form of phase amplitude coupling is increased during cognition and decreased in the SOZ.[27] Theta high-gamma coupling is canonical because both the modulating and the modulated signals are true oscillations. In the case of coupling between epileptiform spike phase and ripple amplitude, the epileptiform spike and ripple are both brief transient events, and furthermore, the spike is not a true oscillation. Coupling due to Gibb's phenomenon, that is, filter ringing,[24] is artifactual or noncanonical, since in this case neither the modulated or modulating signals are true oscillations.[21,22]

The results of the ripple phasor and ripple-triggered averaging methods were also in agreement regarding the preferred phase angle of coupling as near the peak or the trough of the epileptiform spike. This preferred phase angle relates the maximum changes in excitability associated with the interictal discharge to the synchronization of the neuronal assembly generating the pRipple (80–150 Hz). The bimodal distribution of preferred phase angles, near the peak or the trough of the spike, results from the spatial geometry of the dipole relative to the recording electrode. In accord with this concept, we observed shifts of >150 degrees in the preferred phase angle of coupling between mesial contacts and neocortical contacts on the same depth probe. However, we also observed smaller shifts >75° across adjacent electrodes located in mesial temporal structures, suggesting that spike propagation and the cellular and dendritic composition of the tissue adjacent to the macroelectrode contact may also influence the preferred phase angle of coupling.

The ripple phasor method was advantageous in that it was rapid and robust; however, it did not provide information regarding the morphology of the modulating signal or the spectral frequency content of the modulated events. The ripple-triggered averaging method required increased computation, but provided these details.

The ripple-triggered averaging method showed that epileptiform spike phase often modulates ripple, and in some cases, gamma amplitude. The onset of ripple[28] and gamma[29] oscillations can precede interictal epileptiform discharges, whereas gamma can occur after interictal discharges as well as fast ripples, that is, fast-ripple tail gamma.[7] The significance of the gamma oscillations coupled with epileptiform spike phase is unclear, but perhaps may be generated by increased activity among inhibitory interneurons,[30] coordinating a large assembly of synchronized principal neurons to generate the pRipple.[16,19] Alternatively, the co-occurrence of ripple and gamma frequencies during interictal discharges may be coincidental, and the mechanisms generating these two frequencies may be independent.

The strength of coupling between epileptiform spike phase and ripple amplitude is increased in the SOZ

We found that the strength of coupling between epileptiform spike phase and ripple amplitude was increased in the SOZ over NSOZ. In addition, compared to ratios derived from total ripples and ripples on spikes (RonS), for most patients, larger ratios of phase-locked ripple phasors indicated relatively higher rates of ripples coupled with spikes in the SOZ than rates in NSOZ. Although the differences between ratios were small, phase-locked RonS could improve the localization of SOZ in appropriately powered studies. Because only two of the seven patients who underwent resective epilepsy surgery had a sufficient postoperative observation period, that is, >12 months, it remains uncertain if ripples, RonS, and coupled RonS rates can also serve as a biomarker of the epileptogenic zone.

Previous studies showed rates of ripples that were associated with epileptiform spikes irrespective of PAC may,[29,31] or may not,[32] be superior to rates of ripples in the absence of epileptiform spikes to delineate epileptogenic tissue. Differences between these studies could result from possible contamination of ripples with artifact due to the Gibb's phenomenon, especially in recordings that contain epileptiform spikes.[33,34] In the current study, we excluded putative RonS that were most likely produced by filter ringing, and found that in most patients, phase-locked RonS served as a more useful biomarker of the SOZ.

It should also be considered that physiologic sharp-wave ripples may have been misclassified as RonS in our study. However, the specificity of the RonS for the SOZ makes this possibility less likely, since sharp wave ripples occur only in the bilateral hippocampi simultaneously.[19]

Although coupling between epileptiform spike phase and ripple amplitude will require additional studies to determine whether it could be used clinically to help localize the SOZ, the direct correlation between the strength of coupling and

the probability that a macroelectrode site was in the SOZ has important mechanistic implications, since the coupling may be related to the underlying capacity for synchronization[20] among the assembly of neurons generating the pRipple.

Coupling strength influences ripple properties

In recordings from macroelectrodes in the SOZ, greater coupling strength correlated with higher ripple amplitude and lower ripple spectral frequency. It has been demonstrated in studies using computer modeling of normal HFOs[35] and optogenetic manipulation of normal tissue[16] that the larger the size of the HFO-generating network, the lower the spectral frequency of the HFO. Thus, it is possible in epileptogenic tissue that if this relationship holds true, when epileptiform spike phase is strongly coupled with ripple amplitude, a large assembly of synchronized neurons could generate a pRipple that contains spectral power between 80 and 150 Hz.

The pathologically interconnected neuron (PIN) cluster hypothesis[10] predicts that in epileptogenic tissue, very small (1 mm^3) clusters of neurons produce synchronized bursts of action potentials that result in fast pRipples (200–600 Hz). It is possible that the size of a PIN cluster in epileptogenic sites could expand in the context of changes of excitability. This possibility was clearly established in the context of bathing slices of hippocampus from kainic acid–treated rats in the γ-aminobutyric acid receptor A ($GABA_A$) antagonist bicuculline.[10] Perhaps the changes in excitability responsible for the epileptiform spike also cause a massive increase in the size of a synchronized PIN cluster, thereby generating a slower pRipple (80–150 Hz) that occurs at a preferred phase angle. Evidence that ripple frequency oscillations can be pathologic is derived from the findings that they can arise during epileptogenesis in the dentate gyrus that does not usually generate ripple oscillations,[36] and during ictogenesis, in the hippocampus, entorhinal cortex,[37] and neocortex.[38,39]

Clear evidence for synchronized bursting among principal neurons during RonS is lacking. Recordings from single neurons in mesial temporal structures using microelectrodes,[40–43] or calcium imaging,[30] have shown that during interictal discharges, just 20–40% of neurons show a change in firing rate,[30,40,41] that only ~30% of the modulated neurons increase their firing rate or show burst firing,[40,41] and that synchronous firing rarely occurs across regions of 500 μm.[41] Yet, burst firing in principal neurons is known to be phase-locked to the ripple oscillations,[42,43] suggesting that synchronized bursting may indeed occur across more restricted spatial regions.

Summary

Results of interictal phase-locked ripples on epileptiform spikes could reflect that epileptogenic regions exhibiting hyperexcitability responsible for epileptiform spikes also synchronize and enlarge clusters of pathologically bursting neurons manifesting as low-frequency pRipples. Furthermore, these results are also consistent with the hypothesis that interictal phase-locked ripples on spike are a biomarker of the SOZ.

Acknowledgments

We thank Dr. John Stern, Dr. Dawn Eliashiv; and Dr. Christine Bower-Baca for clinical support; Mr. Kirk Shattuck for technical support; and Ms. Sandra Dewar for administrative support.

Funding

Dr. Weiss is supported by an Epilepsy Foundation Award Research and Training Fellowship for Clinicians; Dr. Orosz by the Otfrid-Foerster grant of the German Epilepsy Society; Miss. Van't Klooster by the Ter Meulen Grant of the Royal Netherlands Academy of Arts and Science (KNAW) and the University Utrecht Short Stay PhD Fellowship; Dr. Fried by National Institute of Neurological Disorders and Stroke (NINDS) grant NS033221; Dr. Engel by NS033310; Dr. Staba by NS071048; and Dr. Bragin by NS065877.

Disclosure

The authors declare no conflicts of interest. We confirm that we have read the Journal's position on issues involved in ethical publication and affirm that this report is consistent with those guidelines.

References

1. Engel J, Wiebe S, French J, et al. Practice parameter: temporal lobe and localized neocortical resections for epilepsy. *Epilepsia* 2003;44:741–751.
2. Wiebe S, Blume WT, Girvin JP, et al. A randomized, controlled trial of surgery for temporal-lobe epilepsy. *N Engl J Med* 2001;345:311–318.
3. Engel J Jr, McDermott MP, Wiebe S, et al. Early surgical therapy for drug-resistant temporal lobe epilepsy: a randomized trial. *JAMA* 2012;307:922–930.
4. Engel J Jr, Bragin A, Staba R, et al. High-frequency oscillations: what is normal and what is not? *Epilepsia* 2009;50:598–604.
5. Gotman J. High frequency oscillations: the new EEG frontier? *Epilepsia* 2010;51:63–65.
6. Rosenow F, Lüders H. Presurgical evaluation of epilepsy. *Brain* 2001;124:1683–1700.
7. Bragin A, Engel J Jr, Wilson C, et al. Hippocampal and entorhinal cortex high-frequency oscillations (100–500 Hz) in human epileptic brain and in kainic acid-treated rats with chronic seizures. *Epilepsia* 1999;40:127–137.
8. Staba RJ, Wilson CL, Bragin A, et al. Quantitative analysis of high-frequency oscillations (80–500 Hz) recorded in human epileptic hippocampus and entorhinal cortex. *J Neurophysiol* 2002;88:1743–1752.
9. Bragin A, Wilson CL, Staba RJ, et al. Interictal high-frequency oscillations (80–500 Hz) in the human epileptic brain: entorhinal cortex. *Ann Neurol* 2002;52:407–415.
10. Bragin A, Mody I, Wilson CL, et al. Local generation of fast ripples in epileptic brain. *J Neurosci* 2002;22:2012–2021.
11. Foster DJ, Wilson MA. Reverse replay of behavioural sequences in hippocampal place cells during the awake state. *Nature* 2006;440:680–683.
12. Diba K, Buzsáki G. Forward and reverse hippocampal place-cell sequences during ripples. *Nat Neurosci* 2007;10:1241–1242.
13. Axmacher N, Elger CE, Fell J. Ripples in the medial temporal lobe are relevant for human memory consolidation. *Brain* 2008;131:1806–1817.

14. Lachaux J-P, Axmacher N, Mormann F, et al. High-frequency neural activity and human cognition: past, present and possible future of intracranial EEG research. *Prog Neurobiol* 2012;98:279–301.
15. Ylinen A, Bragin A, Nadasdy Z, et al. Sharp wave-associated high-frequency oscillation (200 Hz) in the intact hippocampus: network and intracellular mechanisms. *J Neurosci* 1995;15:30–46.
16. Stark E, Roux L, Eichler R, et al. Pyramidal cell-interneuron interactions underlie hippocampal ripple oscillations. *Neuron* 2014;83:467–480.
17. Jacobs J, Staba R, Asano E, et al. High-frequency oscillations (HFOs) in clinical epilepsy. *Prog Neurobiol* 2012;98:302–315.
18. Haegelen C, Perucca P, Chatillon CÉ, et al. High-frequency oscillations, extent of surgical resection, and surgical outcome in drug-resistant focal epilepsy. *Epilepsia* 2013;54:848–857.
19. Buzsáki G. Hippocampal sharp wave-ripple: a cognitive marker for episodic memory and planning. *Hippocampus* 2015;25:1073–1188.
20. Canolty RT, Ganguly K, Kennerley SW, et al. Oscillatory phase coupling coordinates anatomically dispersed functional cell assemblies. *Proc Natl Acad Sci U S A* 2010;107:17356–17361.
21. Weiss SA, Banks GP, McKhann GM, et al. Ictal high frequency oscillations distinguish two types of seizure territories in humans. *Brain* 2013;136:3796–3808.
22. Weiss SA, Lemesiou A, Connors R, et al. Seizure localization using ictal phase-locked high gamma: a retrospective surgical outcome study. *Neurology* 2015;84:2320–2328.
23. Perucca P, Dubeau F, Gotman J. Intracranial electroencephalographic seizure-onset patterns: effect of underlying pathology. *Brain* 2014;137:183–196.
24. Bénar CG, Chauvière L, Bartolomei F, et al. Pitfalls of high-pass filtering for detecting epileptic oscillations: a technical note on "false" ripples. *Clin Neurophysiol* 2010;121:301–310.
25. Dvorak D, Fenton AA. Toward a proper estimation of phase–amplitude coupling in neural oscillations. *J Neurosci Methods* 2014;225:42–56.
26. Canolty RT, Knight RT. The functional role of cross-frequency coupling. *Trends Cogn Sci* 2010;14:506–515.
27. Canolty RT, Edwards E, Dalal SS, et al. High gamma power is phase-locked to theta oscillations in human neocortex. *Science* 2006;313:1626–1628.
28. van Klink N, Frauscher B, Zijlmans M, et al. Relationships between interictal epileptic spikes and ripples in surface EEG. *Clin Neurophysiol* 2016;127:143–149.
29. Ren L, Kucewicz MT, Cimbalnik J, et al. Gamma oscillations precede interictal epileptiform spikes in the seizure onset zone. *Neurology* 2015;84:602–608.
30. Muldoon SF, Villette V, Tressard T, et al. GABAergic inhibition shapes interictal dynamics in awake epileptic mice. *Brain* 2015;138:2875–2890.
31. Wang S, Wang IZ, Bulacio JC, et al. Ripple classification helps to localize the seizure-onset zone in neocortical epilepsy. *Epilepsia* 2013;54:370–376.
32. Jacobs J, LeVan P, Chander R, et al. Interictal high-frequency oscillations (80–500 Hz) are an indicator of seizure onset areas independent of spikes in the human epileptic brain. *Epilepsia* 2008;49:1893–1907.
33. Amiri M, Lina J-M, Pizzo F. High frequency oscillations and spikes: separating real HFOs from false oscillations. *Clin Neurophysiol* 2016;127:187–196.
34. Jacobs J, Vogt C, LeVan P, et al. The identification of distinct high-frequency oscillations during spikes delineates the seizure onset zone better than high-frequency spectral power changes. *Clin Neurophysiol* 2016;127:129–142.
35. Brunel N, Brunel N, Wang X-J. What determines the frequency of fast network oscillations with irregular neural discharges? I. Synaptic dynamics and excitation-inhibition balance. *J Neurophysiol* 2003;90:415–430.
36. Bragin A, Wilson CL, Almajano J, et al. High-frequency oscillations after status epilepticus: epileptogenesis and seizure genesis. *Epilepsia* 2003;45:1017–1023.
37. Weiss SA, Alvarado-Rojas C, Bragin A, et al. Ictal onset patterns of local field potentials, high frequency oscillations, and unit activity in human mesial temporal lobe epilepsy. *Epilepsia* 2016;57:111–121.
38. Gnatkovsky V, de Curtis M, Pastori C, et al. Biomarkers of epileptogenic zone defined by quantified stereo-EEG analysis. *Epilepsia* 2014;55:296–305.
39. Fisher RS, Webber WR, Lesser RP, et al. High-frequency EEG activity at the start of seizures. *J Clin Neurophysiol* 1992;9:441–448.
40. Keller CJ, Truccolo W, Gale JT, et al. Heterogeneous neuronal firing patterns during interictal epileptiform discharges in the human cortex. *Brain* 2010;133:1668–1681.
41. Alvarado-Rojas C, Lehongre K, Bagdasaryan J, et al. Single-unit activities during epileptic discharges in the human hippocampal formation. *Front Comput Neurosci* 2013;7:140.
42. Le Van Quyen M, Bragin A, Staba R, et al. Cell type-specific firing during ripple oscillations in the hippocampal formation of humans. *J Neurosci* 2008;28:6104–6110.
43. Alvarado-Rojas C, Huberfeld G, Baulac M, et al. Different mechanisms of ripple-like oscillations in the human epileptic subiculum. *Ann Neurol* 2015;77:281–290.

Supporting Information

Additional Supporting Information may be found in the online version of this article:

Figure S1. Flowchart of iEEG signal processing used to exclude artifact, detect ripple events, derive ripple on spike phasors, and test for coupling between epileptiform spike phase and ripple amplitude.

Figure S2. Illustration of the derivation of individual ripple phasors from intracranial EEG recordings, and the determination of phase locking across the population of ripple phasor events captured during the entire recording epoch.

Figure S3. Distinguishing true ripples on spikes from false ripples on spikes that result from filter ringing.

Figure S4. Mean event rates in the SOZ and NSOZ for each of the 12 patients.

Figure S5. Comparison of ripple on spike properties within (blue) and outside resected brain regions (orange).

Appendix S1. Supplementary methods.